Society of Medical Education & Research

2025, Volume 5, Issue 2, Page No: 13-33
ISSN: 3108-4834

Archive of International Journal of Cancer and Allied Science

CircDLG1 Drives Anti-PD-1 Resistance and Gastric Cancer Progression via the miR-141-3p/CXCL12 Axis

Emily Carter[1], Daniel J. Morris[2]*, Hannah Lee[1], Robert Thompson[2]

[1] Department of Clinical Oncology, Faculty of Medicine, University of Toronto, Toronto, Canada.
[2]Department of Cancer Epidemiology, School of Public Health, McGill University, Montreal, Canada.

***E-mail** ✉ daniel.morris@outlook.com

Abstract

Increasing evidence indicates that abnormal circRNA expression contributes significantly to gastric cancer progression; therefore, understanding the underlying biological roles and molecular mechanisms of these dysregulated circRNAs is essential for the discovery of novel therapeutic strategies. To screen for circRNAs associated with metastasis and immunotherapy response in gastric cancer, a circRNA expression profiling analysis was performed on primary tumors, distant metastatic lesions, and tumor samples exhibiting either sensitivity or resistance to anti–PD-1 treatment. Based on this analysis, circDLG1 expression was further examined in an independent and larger collection of gastric cancer specimens. Functional experiments were carried out to determine the contribution of circDLG1 to malignant progression using both cell-based models and animal studies. In addition, the influence of circDLG1 on the therapeutic efficacy of PD-1 blockade was assessed in vivo. The molecular interaction between circDLG1 and miR-141-3p was validated through RNA immunoprecipitation combined with reporter gene assays. CircDLG1 expression was markedly elevated in metastatic gastric cancer lesions and in tumors that failed to respond to PD-1 blockade, and its high expression correlated with aggressive clinicopathological features and poor outcomes in patients receiving anti-PD-1 therapy. Forced overexpression of circDLG1 enhanced gastric cancer cell growth, motility, invasiveness, and immune escape capabilities. At the mechanistic level, circDLG1 directly bound miR-141-3p, functioning as a competing endogenous RNA that relieved miR-141-3p–mediated repression of CXCL12, thereby facilitating tumor progression and diminishing sensitivity to PD-1–targeted immunotherapy. Collectively, these results reveal that circDLG1 enhances malignant behaviors—including cellular growth, motility, invasiveness, and immune escape—in gastric cancer, and highlight a previously unrecognized contribution of circRNAs to the molecular mechanisms driving gastric cancer progression.

Keywords: Immune evasion, Gastric cancer, circDLG1, Invasion, Proliferation

Introduction

Gastric cancer remains one of the most frequently diagnosed malignancies and a leading contributor to cancer-related mortality worldwide [1]. Despite notable advances in therapeutic approaches over recent years, patient outcomes—particularly for those with advanced disease—remain unsatisfactory. Disease progression and the development of distant metastases represent the primary causes of mortality. For individuals with metastatic gastric cancer, systemic chemotherapy continues to be the cornerstone of treatment. Accumulating evidence has highlighted immune escape as a critical mechanism enabling tumor survival and progression [2, 3]. Within the tumor microenvironment, cancer cells are capable of recruiting immunosuppressive cell populations, including $CD4^+$ T cells, which impair the cytotoxic activity of $CD8^+$ T cells [4, 5]. Furthermore, programmed death ligand 1 (PD-L1), a member of the B7 ligand family, can interact with its receptor programmed death 1 (PD-1) on T cells, leading to T-cell apoptosis and functional inhibition of $CD8^+$ T cells, thereby facilitating tumor immune evasion. Clinically, blockade of the PD-1

Access this article online https://smerpub.com/

Received: 08 May 2025; **Accepted:** 11 August 2025

How to cite this article: Carter E, Morris DJ, Lee H, Thompson R. CircDLG1 Drives Anti-PD-1 Resistance and Gastric Cancer Progression via the miR-141-3p/CXCL12 Axis . Arch Int J Cancer Allied Sci. 2025;5(2):13-33. https://doi.org/10.51847/snq9DXS1f2

immune checkpoint using monoclonal antibodies has emerged as an effective immunotherapeutic strategy across multiple cancer types [6, 7]. Our previous work has also demonstrated the clinical benefit of PD-1 antibody therapy in patients with gastric cancer [8]. Nevertheless, the majority of gastric cancer patients exhibit primary or acquired resistance to anti-PD-1 treatment, with durable responses observed in only a subset of individuals [9]. Although PD-L1 expression has been validated as a predictive biomarker for PD-1 blockade efficacy in several malignancies, its prognostic and predictive value in gastric cancer remains controversial [10]. The KEYNOTE-061 and KEYNOTE-062 trials reported improved survival outcomes in patients with PD-L1–positive tumors treated with pembrolizumab [11, 12]. In contrast, results from the CheckMate 032, JAVELIN Gastric 300, and ATTRACTION-2 studies did not support PD-L1 expression as a reliable predictor of response to anti-PD-1 therapy [13–15]. Consequently, elucidating the molecular mechanisms underlying gastric cancer progression and immune escape is essential for improving therapeutic strategies.

Circular RNAs (circRNAs) represent a recently characterized class of noncoding or protein-coding RNAs distinguished by their covalently closed-loop structures, lacking 5′–3′ polarity and polyadenylated tails [16]. These molecules are predominantly generated through back-splicing of precursor mRNA transcripts and are mainly localized within the cytoplasm [17, 18]. circRNAs have been shown to be highly stable, evolutionarily conserved, and abundantly expressed across various tumor types and tissues [19]. A growing body of research indicates that circRNAs play key roles in diverse biological and pathological processes, including gene regulation, apoptosis, cell-cycle control, migration, and invasion [20]. In our earlier work, we identified a circRNA-based signature capable of predicting postoperative recurrence in patients with stage II–III colon cancer [21]. Mechanistically, circRNAs exert their functions through multiple modes of action, such as acting as microRNA sponges, interacting with RNA-binding proteins, or encoding functional peptides [22–24]. For example, we previously demonstrated that circUBXN7 was downregulated in bladder cancer, and that enforced circUBXN7 expression inhibited tumor cell proliferation and invasion by sequestering miR-1247 and upregulating B4GALT3 expression [25]. Rong *et al*. [26] reported that circPSMC3 suppresses gastric cancer cell proliferation and metastasis, while Han *et al*. [27] showed that circMTO1 regulates hepatocellular carcinoma progression by sponging miR-9 to modulate p21 expression. Additionally, Hsiao *et al*. [28] demonstrated that circCCDC66 facilitates colon cancer progression and metastasis. Despite these advances, the contribution of circRNAs to gastric cancer progression and immune evasion remains incompletely understood.

In the present study, we sought to identify circRNAs involved in gastric cancer progression and immune escape by performing circRNA microarray analyses on primary tumors, distant metastatic lesions, and tumor tissues exhibiting sensitivity or resistance to anti-PD-1 therapy. Our results revealed that circDLG1 (hsa_circ_0008583), a circRNA derived from the DLG1 gene, was markedly upregulated in metastatic samples and in primary gastric cancer tissues resistant to PD-1 blockade. Importantly, elevated circDLG1 expression was closely associated with aggressive tumor characteristics and unfavorable clinical outcomes in gastric cancer patients receiving anti-PD-1 treatment. Functional experiments demonstrated that ectopic circDLG1 expression enhanced gastric cancer cell proliferation, invasion, and immune evasion in vitro, as well as tumor growth and metastatic potential in immunocompetent mouse models in vivo. Mechanistic investigations further showed that circDLG1 directly binds to miR-141-3p, functioning as a competing endogenous RNA to derepress the miR-141-3p target gene chemokine ligand 12 (CXCL12), thereby driving gastric cancer progression. Collectively, these findings suggest that circDLG1 may serve as a novel biomarker and potential therapeutic target in gastric cancer.

Materials and Methods

Human cell lines and tissue samples

Tumor specimens preserved by freezing or paraffin embedding were collected from patients with advanced gastric carcinoma treated at Sun Yat-sen University Cancer Center who received PD-1 inhibitor therapy following diagnostic gastroscopy with biopsy, needle aspiration biopsy, or palliative surgical intervention between August 2018 and October 2019. All patients were prospectively enrolled in a real-world investigation assessing PD-1 antibody–based immunotherapy in gastric cancer (ClinicalTrials.gov registration number: NCT04086888). The study cohort consisted of 126 individuals diagnosed with gastric cancer. Primary tumor

material was obtained from 82 patients. Treatment response to PD-1 blockade could be evaluated in 73 cases, among which tissue samples from 30 patients were available for analysis, including samples from primary tumors, matched non-malignant gastric tissues, and distant metastatic sites. Clinical response assessments were conducted at intervals of three to four treatment cycles, and patients were monitored continuously throughout therapy. Tumor responses were classified in accordance with RECIST version 1.1 as complete response, partial response, stable disease, or progressive disease. The objective response rate was defined as the proportion of patients achieving complete or partial tumor regression. Demographic and clinicopathological variables—including age, sex, tumor diameter, histological grade, peritoneal dissemination status, and Lauren classification—were obtained from institutional medical records. Ethical approval for the study was granted by the Ethics Committee of Sun Yat-sen University Cancer Center, and informed consent was obtained from all participants prior to inclusion. Overall survival was defined as the time from initiation of PD-1 inhibitor therapy to death or last follow-up, while progression-free survival was calculated from treatment initiation to documented disease progression or death.

A panel of human gastric carcinoma cell lines (BGC823, HGC27, MKN28, MKN45, AGS and SGC7901), along with the non-malignant gastric epithelial cell line GES-1, the murine gastric cancer cell line MFC, and HEK293T cells, was obtained from the Shanghai Institute of Cell Biology, Chinese Academy of Sciences (Shanghai, China). All cell lines were propagated under standard conditions specified by the supplier.

CircRNA microarray analysis

To screen for circRNAs potentially associated with gastric cancer progression and resistance to PD-1 blockade, tumor samples were selected from a subset of patients with distinct therapeutic outcomes. This cohort included three patients who achieved partial responses to anti-PD-1 treatment and exhibited progression-free survival exceeding 10 months, as well as six patients who failed to respond to therapy—comprising two cases of stable disease and four cases of progressive disease—with progression-free survival durations shorter than 5 months. These samples were subjected to circRNA expression profiling.

Microarray experiments were carried out by Kangchen Biotech (Shanghai, China). Sample processing and hybridization procedures were performed in accordance with the manufacturer's protocols provided by Arraystar (Rockville, MD, USA). Briefly, total RNA was treated with RNase R to selectively degrade linear RNA species, thereby enriching circular RNA molecules. The resulting circRNA-enriched fractions were subsequently amplified and labeled with fluorescent complementary RNA using random priming (Arraystar Super RNA Labeling Kit). Labeled products were hybridized to the Human circRNA Array V2 platform (8 × 15K, Arraystar). Following hybridization, microarrays were scanned using the Agilent G2505C scanner, and raw data were extracted using Agilent Feature Extraction software (version 11.0.1.1). Differential circRNA expression was determined using a random variance statistical model, with paired t-tests applied for significance testing. circRNAs displaying an absolute fold change of at least 2.0 and a P value of 0.05 or lower were considered significantly differentially expressed.

Quantitative real-time PCR (qRT–PCR)

Total RNA was extracted from gastric cancer tissues and cell lines using TRIzol reagent (Sigma–Aldrich, St. Louis, MO, USA) in accordance with the manufacturer's instructions. Complementary DNA synthesis was performed using random primers for mRNA and stem–loop primers for miRNA. Quantitative PCR was conducted on a Bio–Rad CFX96 platform with TaqMan Universal Master Mix II. Relative RNA expression was calculated using the $2^{-\Delta\Delta}$CT method. For subcellular localization analyses, cytoplasmic and nuclear fractions were separated using the PARIS Kit (Life Technologies), and RNA was isolated from each compartment. The distribution of specific RNAs between nucleus and cytoplasm was then determined by qRT–PCR, with GAPDH serving as a cytoplasmic control and U6 as a nuclear control.

Western blotting

Protein expression was assessed by Western blot as described previously [29]. Total protein was extracted from concentrations and gastric cancer cell line were quantified using the Pierce BCA Protein Assay Kit (Thermo Scientific, Rockford, IL, USA). Proteins were then separated by SDS-PAGE, transferred to membranes, and probed with the following primary antibodies: anti-CXCL12 (CST, #3740S) and anti-GAPDH (CST, #2118 L).

Immunohistochemistry (IHC)

IHC staining was carried out following previously established protocols [30]. Paraffin-embedded tumor tissues were sectioned at 4 μm thickness. Images of stained sections were captured with a Leica microscope (Leica, Germany). Two pathologists independently evaluated the staining, and the proportion of positively stained tumor cells was recorded. Anti-CXCL12 (CST, 97958S; 1:200), antibodies used included anti-PD-L1 (22C3 pharmDX; Dako, Carpinteria, CA, USA), and anti-CD33 (clone PWS44; Leica Biosystems, 1:200). PD-L1 expression was considered positive if membrane staining was detected in ≥1% of tumor cells or tumor-infiltrating immune cells. High and low PD-L1 expression groups were defined based on the median expression value.

Flow cytometry

Flow cytometry was performed following previously established methods [31]. The panel of antibodies included anti-mouse IFNγ (BD Biosciences), CD45 (BD Biosciences), Gr-1 (TONBO Biosciences), Ly6G (TONBO Biosciences), Ly6C (BD Biosciences), CD11b (TONBO Biosciences), F4/80 (BioLegend), and the human-specific antibodies CD11b (TONBO Biosciences), CD33 (BD Biosciences), and HLA-DR (BD Biosciences). Cells were first dissociated into single-cell suspensions, washed with PBS, and resuspended in a stabilizing buffer (BioLegend, Cat. No. 420201). Following centrifugation at 350 × g for 5 minutes and removal of the supernatant, 5 μL of Fc receptor blocking solution (Human TruStain FcX™, BioLegend Cat. No. 422301) was added together with the appropriate antibodies and incubated at room temperature for 15–20 minutes. Flow cytometric analysis was then performed. For intracellular IFNγ detection, cells were fixed with BioLegend fixation buffer (Cat. No. 420801) for 20 minutes, washed with intracellular staining perm wash buffer (Cat. No. 421002), incubated with the IFNγ antibody for 20 minutes, and finally analyzed by flow cytometry.

Fluorescence in situ hybridization (FISH)

FISH experiments were carried out as described previously [25]. Cells were incubated with a Cy3-labeled probe targeting circDLG1 and a Cy5-labeled probe targeting miR-141-3p (GenePharma, China) for 12 hours at 37°C. Nuclei were stained with DAPI (Yeasen, Shanghai, China). Imaging and signal capture were performed using a ZEISS LSM800 confocal microscope (Carl Zeiss AG, Germany).

Migration, colony formation, proliferation, and invasion assays

Cell proliferation was assessed using the colony formation assays and CCK-8 assays were conducted to evaluate long-term proliferative capacity. Invasion and transwell migration assays were carried out to determine cell motility and invasiveness. Detailed experimental procedures for these assays have been described previously [32].

Luciferase reporter assays and RNA immunoprecipitation (RIP)

RIP experiments were performed using the Magna RIP RNA-Binding Protein Immunoprecipitation Kit (Millipore, USA) following the manufacturer's guidelines. Briefly, cell lysates were incubated with Dynabeads conjugated to either a control IgG antibody (Millipore, USA) or an AGO2-specific antibody (Cell Signaling Technology, USA) for 12 hours at 4°C. RNA associated with the immunoprecipitated complexes was then isolated and analyzed by qRT–PCR to quantify circDLG1 and relevant miRNAs.

Luciferase reporter assays were conducted to validate predicted miRNA binding sites, identified via TargetScanHuman 7.2. and StarBase v3.0 Gastric cancer cells were co-transfected with constructs containing the CXCL12 3′-UTR or pGL-luc-circDLG1 fused to luciferase, along with either negative control mimics or miR-141-3p mimics. After 48 hours, luciferase activity was measured using the Dual-Luciferase Reporter Assay System (Promega, USA) according to the manufacturer's instructions.

Overexpression and circDLG1 knockdown

shRNAs specifically targeting the circDLG1 back-splice junction and a lentiviral circDLG1 overexpression vector were synthesized by Geneseed Biotech Co., Ltd. (Guangzhou, China). Gastric cancer cell lines were transfected with these constructs according to the manufacturer's protocol, as previously reported [25].

In vivo metastasis assays and tumor growth

All animal procedures were approved by the Animal Experiment Ethics Committee of Sun Yat-sen University Cancer Center. BALB/c nude and C57BL/6 mice were obtained from the Shanghai Institute of Material

Medicine (Shanghai, China) and maintained under standard laboratory conditions. The experimental procedures followed our prior study [33].

To examine tumorigenic potential, MFC cells expressing circDLG1 shRNA (MFC-sh-circDLG1) or control shRNA (MFC-sh-NC) were injected subcutaneously into the flanks of mice at a dose of 1 × 10^6 cells per mouse, with ten mice per group. Tumor growth was monitored every four days, and volumes were calculated. After four weeks, mice were euthanized, and tumors were harvested for analysis.

For metastasis studies, MFC-sh-circDLG1 or MFC-sh-NC cells (2 × 10^6 cells per mouse) were introduced via tail vein injection into separate groups of mice (ten per group). Four weeks post-injection, mice were sacrificed, lungs were collected, and tissue samples were paraffin-embedded. Serial 4-μm sections were prepared, stained with hematoxylin and eosin, and micrometastases were enumerated under a dissecting microscope.

In vivo anti-PD-1 xenograft study

To assess CXCL12's impact on tumor immune evasion and response to PD-1 blockade, subcutaneous xenograft experiments were performed in C57BL/6 mice. Mice were divided into experimental groups and injected in the left flank with either MFC cells expressing control shRNA (MFC-sh-NC) or CXCL12-targeting shRNA (MFC-sh-CXCL12), with ten mice per group (1×10^6 cells per mouse). MFC-sh-NC tumor-bearing mice received one of the following interventions: saline (0.9% NS), anti-PD-1 antibody, AMD3100 (a CXCR4 inhibitor), or a combination of anti-PD-1 and AMD3100 antibody. MFC-sh-CXCL12 xenografts were treated with either saline or anti-PD-1 antibody. The mouse anti-PD-1 antibody was sourced from Bio X Cell (West Lebanon, NH, USA), and AMD3100 was obtained from Selleck (Shanghai, China) and prepared in PBS. Treatments were delivered via intraperitoneal injection according to previously described procedures [34]. Mice were sacrificed four weeks after treatment initiation or earlier if they showed signs of severe distress. Survival duration was calculated from the day of the first administration until euthanasia.

Statistical methods

All measurements are reported as mean ± standard deviation unless otherwise indicated. Statistical evaluations were carried out using GraphPad Prism 7 (GraphPad Software, La Jolla, CA, USA) or SPSS 17.0 (SPSS Inc., Chicago, IL, USA). Differences between groups were analyzed using Student's t-test, chi-square test, or one-way ANOVA as appropriate. Pearson correlation analysis was applied to assess relationships between variables. Progression-free survival was calculated using the Kaplan–Meier method with log-rank testing, and Cox proportional hazards models were employed to identify independent prognostic factors. A P-value < 0.05 was considered statistically significant.

Results and Discussion

Identification of circRNAs associated with immune evasion and gastric cancer progression

To explore circRNAs potentially involved in immune escape and gastric cancer progression, we conducted a circRNA microarray analysis using nine paired gastric cancer specimens, including primary tumors and matched distant metastatic lesions, from patients treated with anti-PD-1 therapy. A circus plot was generated to illustrate the chromosomal distribution and expression patterns of the detected circRNAs, as well as their predicted miRNA interactions **(Figure 1a).** The heatmap highlights the circRNAs showing significant differential expression between primary tumors and paired metastatic tissues **(Figure 1b).**

To pinpoint circRNAs potentially linked to anti-PD-1 resistance, we compared circRNA profiles in primary tumors from three patients who responded to therapy (partial response, PR) and four patients who were nonresponsive (progressive disease, PD) to anti-PD-1 treatment **(Figure 1c).** CircRNAs that were upregulated both in metastatic lesions and in tissues from anti-PD-1-resistant patients—hsa_circ_0008583 and hsa_circ_0002387—were identified. Among these, only hsa_circ_0008583, originating from exons 13–16 of the DLG1 gene and hereafter referred to as circDLG1, was consistently upregulated in metastatic lesions and primary tumors resistant to anti-PD-1 in a larger patient cohort **(Figures 1d and 1 e).** In addition, circDLG1 levels were elevated in primary tumors compared with adjacent normal tissues, though the difference did not reach statistical significance.

Kaplan–Meier survival analysis revealed that high circDLG1 expression was associated with shorter progression-free survival (PFS) in gastric cancer patients receiving anti-PD-1 therapy, whereas patients with lower circDLG1 expression exhibited a significantly better prognosis **(Figure 1f).** Patients were stratified into high-

and low-expression groups according to the mean circDLG1 level determined by qRT–PCR. Notably, circDLG1 expression correlated significantly with tumor size and peritoneal metastasis, but no significant relationships were observed with sex, age, tumor cell differentiation, or Lauren classification.

Given previous reports linking tumor mutation burden (TMB) and PD-L1 expression to anti-PD-1 response in gastric cancer [8, 9], we investigated whether circDLG1 levels were associated with these parameters. RNA in situ hybridization (ISH) confirmed circDLG1 expression in gastric cancer tissues (with blue staining indicating positive expression and red indicating negative), while immunohistochemistry (IHC) was used to assess PD-L1 levels **(Figure 1g).** No significant correlations were observed between circDLG1 expression and either PD-L1 levels or TMB **(Figures 1h and 1i).**

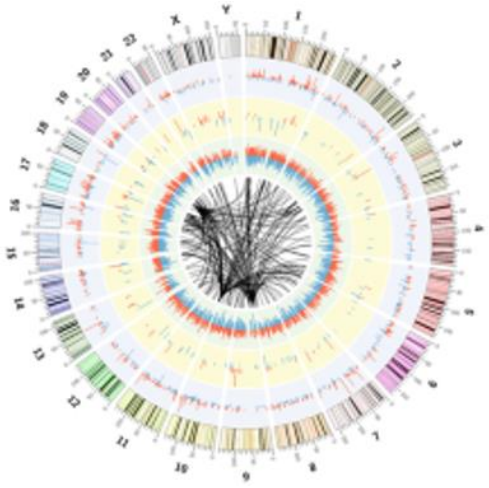

a)

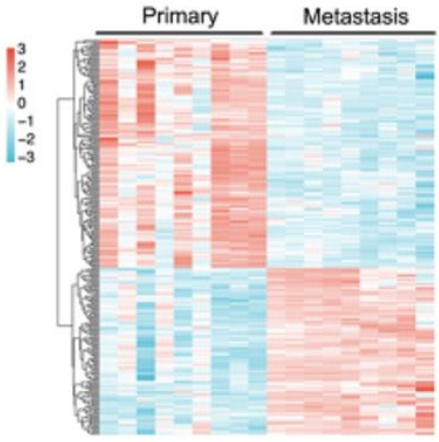

b)

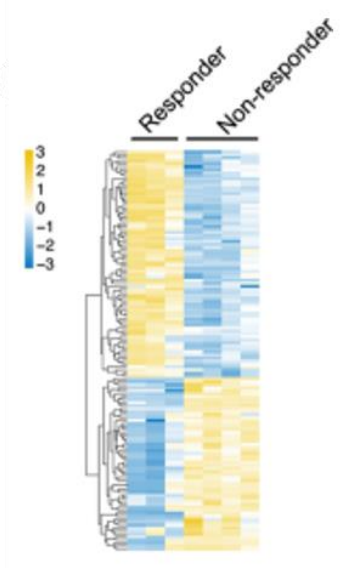

c)

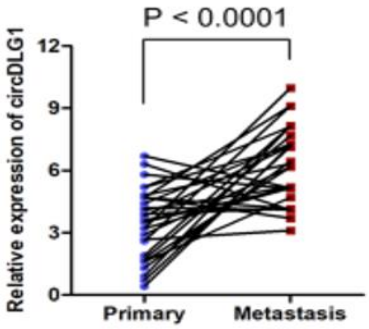

d)

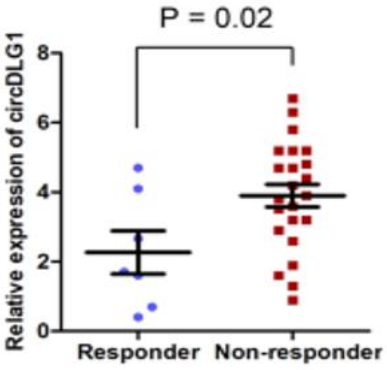

e)

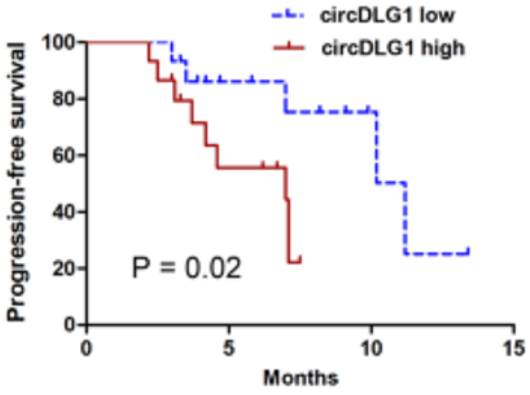

f)

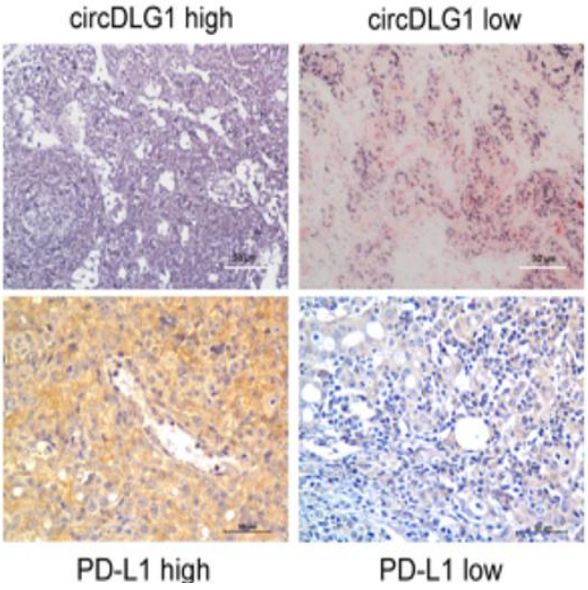

g)

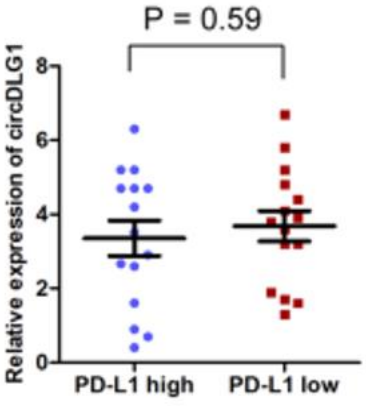

h)

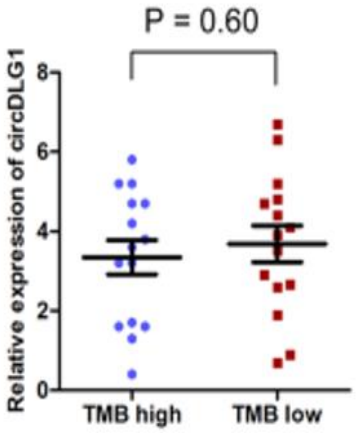

i)

Figure 1. Identification of circRNAs linked to immune evasion and gastric cancer progression via microarray analysis.

a A circRNA microarray was conducted to detect circRNAs differentially expressed in gastric cancer tissues. The circus plot illustrates the chromosomal distribution and expression patterns of the detected circRNAs, highlighting potential miRNA interactions (inner layer, mRNAs; middle layer, miRNAs; outer layer, circRNAs). b Heatmap showing circRNAs with significant differential expression between primary tumors and matched distant metastatic tissues (n = 9). c Heatmap depicting circRNAs with differential expression in primary gastric tumors that were either responsive (n = 3) or resistant (n = 4) to anti-PD-1 therapy. d qRT–PCR analysis of circDLG1 expression in primary and distant metastatic gastric cancer tissues (n = 30; P < 0.001). Expression levels were calculated using the 2^-ΔΔCT method. Statistical significance was determined by Student's t-test. Data represent three technical replicates. e Relative circDLG1 expression in primary tumors from anti-PD-1-responsive (n = 7) and resistant (n = 23) patients (P = 0.002), measured by qRT–PCR using the 2^-ΔΔCT method. Paired Student's t-test was applied. Data represent three technical replicates. f Patients were stratified into circDLG1 high-expression (n = 15) and low-expression (n = 15) groups according to the median circDLG1 level. Kaplan–Meier analysis revealed significantly shorter progression-free survival for patients with elevated circDLG1 compared with those with low expression (P = 0.02). g ISH for circDLG1 (blue, positive; red, negative) and IHC for PD-L1 in gastric cancer tissues. Scale bar, 50 μm. h Comparison of circDLG1 expression between PD-L1

high and PD-L1 low groups by qRT–PCR (P = 0.59), using the 2^-ΔΔCT method and Student's t-test. i circDLG1 expression in tumors with high versus low TMB levels, measured by qRT–PCR (P = 0.60). Expression levels were calculated using the 2^-ΔΔCT method, and Student's t-test was used for comparison.

Overall, these findings suggest that circDLG1 may play a critical role in gastric cancer progression and the modulation of immune evasion.

Characterization of circDLG1 in gastric cancer

Based on data from UCSC genome browser and the circBase database, circDLG1 (hsa_circ_0008583) originates from exons 13–16 of the DLG1 gene, is located on chromosome 3, and spans 496 nucleotides **(Figure 2a).** Divergent primers were used to amplify circDLG1, and its sequence was validated by Sanger sequencing in SGC7901 and AGS gastric cancer cell lines **(Figure 2b)**. PCR amplification was performed on both cDNA and genomic DNA (gDNA), revealing that divergent primers produced detectable products only from cDNA, confirming the circular nature of circDLG1 **(Figure 2b).**

To further characterize circDLG1, reverse transcription was carried out using either random hexamers or oligo(dT)18 primers. When oligo(dT)18 was used, circDLG1 expression decreased markedly, whereas DLG1 mRNA levels remained largely unchanged **(Figure 2c),** indicating that circDLG1 lacks a polyadenylated tail. Moreover, treatment with RNase R, an exonuclease that degrades linear RNAs while sparing circular RNAs, showed that circDLG1 was resistant, whereas DLG1 mRNA was effectively degraded **(Figure 2d).**

To assess transcript stability, SGC7901 cells were treated with actinomycin D, an inhibitor of transcription, and RNA was collected at designated time points. Analysis revealed that circDLG1 exhibited a considerably longer half-life compared with DLG1 mRNA **(Figure 2e).** In addition, subcellular localization studies using qRT–PCR and FISH demonstrated that circDLG1 predominantly resides in the cytoplasm **(Figures 2f and 2g).**

Taken together, these findings indicate that circDLG1 is a stable, cytoplasm-enriched circular RNA with abundant expression in gastric cancer cells.

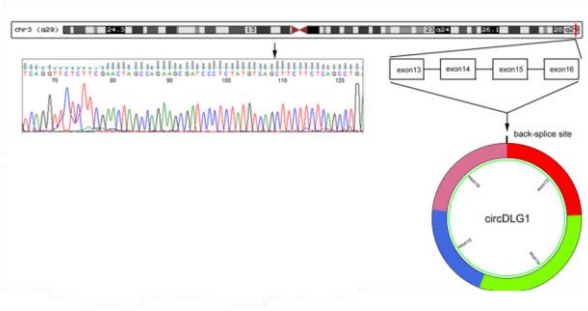

a)

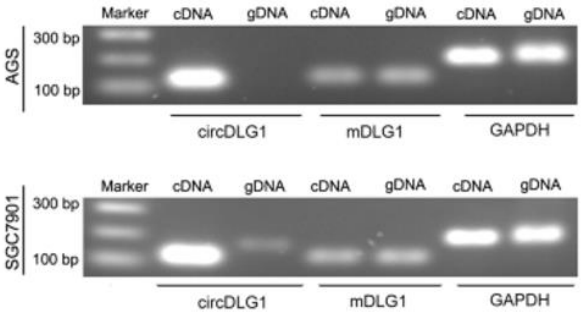

b)

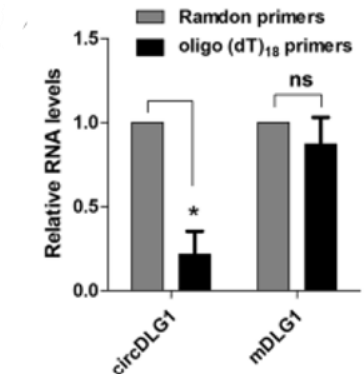

c)

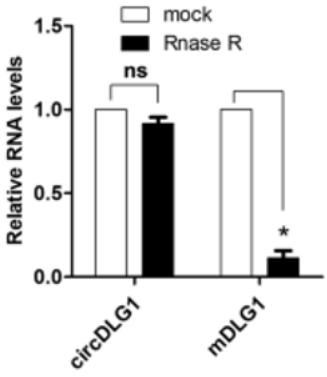

d)

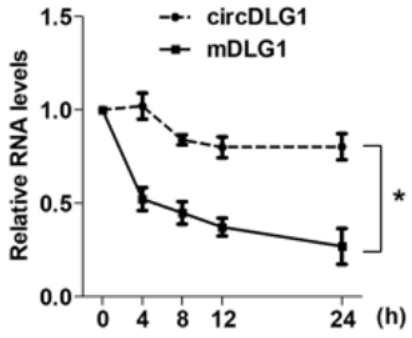

e)

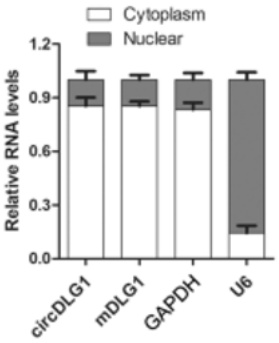

f)

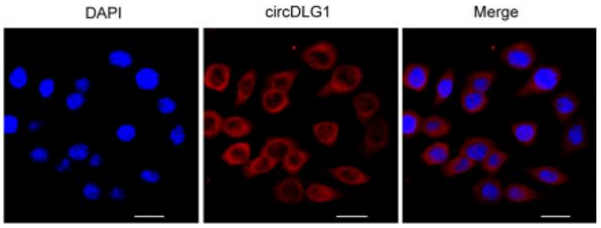

g)

Figure 2. Characterization of circDLG1 in gastric cancer.

a Diagram illustrating the biogenesis of circDLG1. b CircDLG1 was amplified using RT–PCR, and the back-splice junction was verified through Sanger sequencing. Its expression was confirmed in SGC7901 and AGS cell lines, with GAPDH used as a control for linear RNA. c Reverse transcription was performed with either random hexamer or oligo(dT)18 primers. Relative RNA levels were quantified by qRT–PCR and normalized to the random hexamer condition. *P < 0.05, Student's t-test; experiments repeated three times. d qRT–PCR analysis of RNA following RNase R digestion, normalized to untreated AGS cells. *P < 0.05, Student's t-test; three independent replicates. e Time-course qRT–PCR measurement of circDLG1 and DLG1 mRNA in SGC7901 cells treated with actinomycin D. *P < 0.05, two-way ANOVA; three independent experiments. f Nuclear and cytoplasmic fractionation showing the distribution of circDLG1 and DLG1 mRNA, with GAPDH and U6 serving as cytoplasmic and nuclear markers, respectively. g RNA FISH analysis displaying circDLG1 localization in the cytoplasm of SGC7901 cells. Nuclei were stained with 20 μm, DAPI. Scale bar. Data represent three independent experiments.

Invasion and CircDLG1 enhances gastric cancer cell growth

To determine the functional role of circDLG1, its expression was compared across several gastric cancer cell lines and the normal gastric epithelial line GES-1. CircDLG1 was consistently elevated in cancer cells relative to GES-1 **(Figure 3a).** Three shRNAs targeting the unique back-splice junction (sh-1, sh-2, sh-3) were designed, all of which efficiently reduced circDLG1 levels in SGC7901 and HGC27 cells **(Figure 3b).**

Functional assays demonstrated that reducing circDLG1 impaired proliferation and colony formation in both SGC7901 and HGC27 cells, as evidenced by colony formation and CCK-8 assays **(Figures 3c and d).** Similarly, transwell experiments indicated that circDLG1 knockdown strongly suppressed cellular invasion **(Figure 3e).**

Given the key role of epithelial-mesenchymal transition (EMT) in cancer progression, we assessed the effect of circDLG1 on EMT and stemness. Immunofluorescence analysis revealed that depletion of circDLG1 increased E-cadherin and reduced N-cadherin expression **(Figure 3f)**. Consistently, qRT–PCR showed elevated epithelial markers (α-catenin, E-cadherin, β-catenin) and decreased mesenchymal markers (vimentin, N-cadherin, Snail, Slug) following circDLG1 knockdown **(Figure 3g).** In tissue samples, IHC confirmed lower E-cadherin and higher vimentin in tumors with high circDLG1 expression.

Sphere formation assays further demonstrated that silencing circDLG1 diminished the self-renewal capacity of gastric cancer cells **(Figure 3h).** Correspondingly, stemness-associated genes including Oct4, CD24, CD44, CD133, CD155, CD166, Sox2 and Nanog were downregulated upon circDLG1 knockdown (**Figure 3i**). Overall, these findings suggest that circDLG1 drives gastric cancer progression by promoting invasion, proliferation, stemness and EMT.

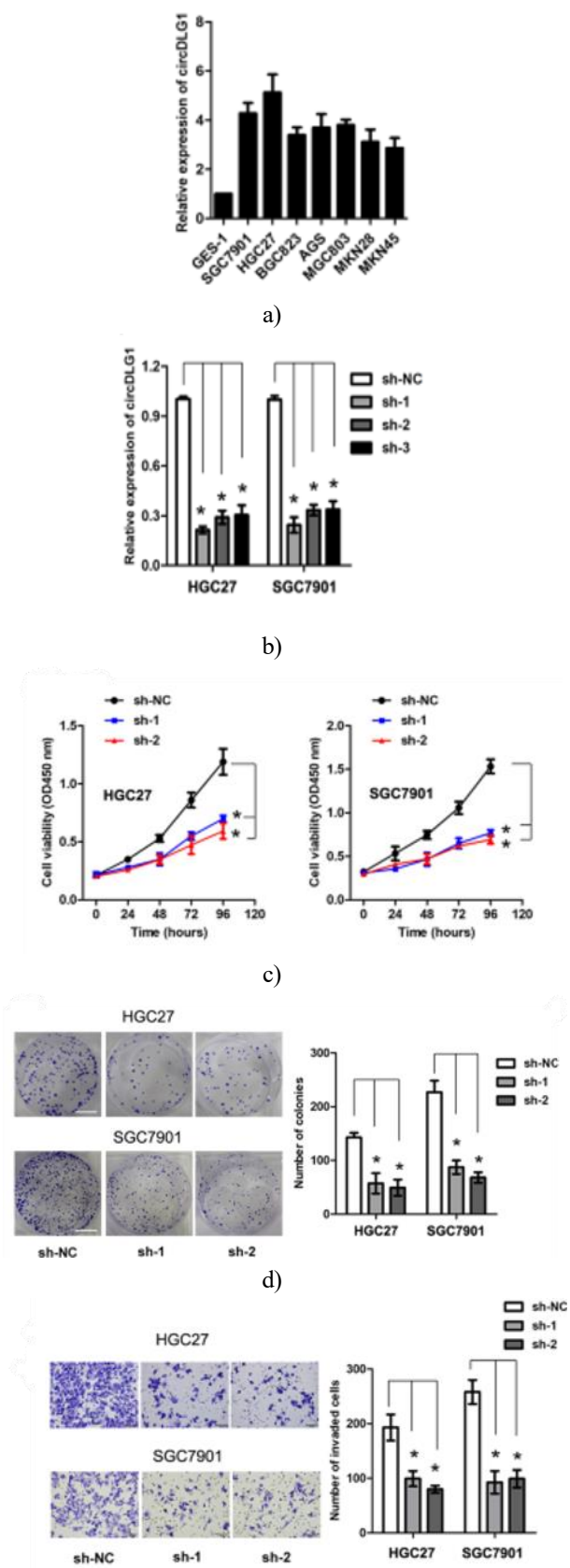

Figure 3. CircDLG1 drives gastric cancer progression. a qRT–PCR analysis comparing circDLG1 levels across multiple gastric cancer cell lines and the normal gastric epithelial line GES-1. b circDLG1 expression in HGC27 and SGC7901 cells after transfection with shRNAs targeting circDLG1 (sh-1, sh-2, sh-3) or negative control (sh-NC), quantified by qRT–PCR. *P < 0.05, one-way ANOVA with Bonferroni-adjusted Student's t-test for individual comparisons; three independent experiments. c Cell proliferation of SGC7901 and HGC27 cells following circDLG1 knockdown, assessed using CCK-8 assays. *P < 0.05, two-way ANOVA with Bonferroni correction. Three independent experiments

performed. d Colony formation ability of HGC27 and SGC7901 cells after circDLG1 silencing. *P < 0.05, one-way ANOVA followed by Bonferroni-adjusted Student's t-tests; three independent experiments. Scale bar, 50 μm. e Transwell assays evaluating cell invasiveness in circDLG1-depleted HGC27 and SGC7901 cells. *P < 0.05, one-way ANOVA with Student's t-test comparing each shRNA to sh-NC; Bonferroni adjustment applied. Experiments repeated three times. Scale bar, 100 μm. f Immunofluorescence imaging showing changes in E-cadherin and N-cadherin expression following circDLG1 knockdown in SGC7901 cells. Scale bar, 50 μm. g qRT–PCR quantification of mesenchymal (N-cadherin, vimentin, Snail, Slug) and epithelial (E-cadherin, α-catenin, β-catenin) markers in SGC7901 cells after circDLG1 depletion. *P < 0.05, **P < 0.01, Student's t-test; three independent experiments. h Sphere formation assay in HGC27 and SGC7901 cells with circDLG1 knockdown. *P < 0.05, **P < 0.01, Student's t-test; three replicates. Scale bar, 100 μm. i qRT–PCR measurement of stemness-associated genes (CD44, CD133, Oct4, CD24, CD155, CD166, Nanog, Sox2) following circDLG1 knockdown in SGC7901 cells. *P < 0.05, **P < 0.01, Student's t-test; experiments repeated three times.

CircDLG1 enhances tumor progression by recruiting MDSCs

To examine circDLG1's contribution to tumor growth in vivo, MFC murine gastric cancer cells were stably transduced with shRNA vectors targeting circDLG1 (MFC-sh-circDLG1). qRT–PCR verified efficient suppression of circDLG1 in these cells.

MFC-sh-circDLG1 cells were introduced into immunocompetent mice either subcutaneously or via tail vein injection. Tumors derived from circDLG1-depleted cells exhibited slower growth and reduced metastatic spread compared with controls **(Figure 4a).** Notably, in immunodeficient mice, circDLG1 knockdown did not significantly affect tumor growth or metastasis **(Figure 4b),** suggesting that its tumor-promoting effect may depend on interactions with the immune system.

IHC analysis of tumors revealed that circDLG1 depletion increased $CD8^+$ T cell infiltration while decreasing $Gr\text{-}1^+$ and $CD11b^+$ MDSCs, key markers of murine myeloid-derived suppressor cells **(Figure 4c)**. Flow cytometry confirmed these findings, showing elevated $CD8^+$ T cells and $IFN\gamma^+$ cells, alongside reduced total MDSCs and granulocytic MDSCs, in circDLG1-silenced tumors **(Figure 4d).**

Analysis of human gastric cancer tissues revealed a positive correlation between circDLG1 expression and $CD33^+$ MDSC infiltration, supporting the relevance of this mechanism in patients **(Figures 4e and 4f).**

Together, these observations indicate that circDLG1 facilitates gastric cancer progression at least in part by enhancing MDSC recruitment, thereby contributing to immune evasion.

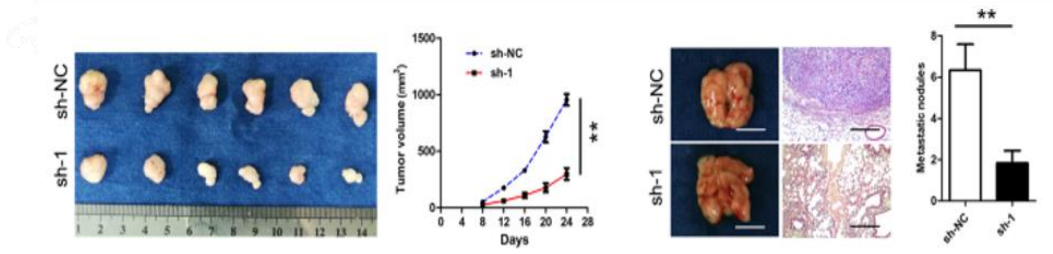

a)

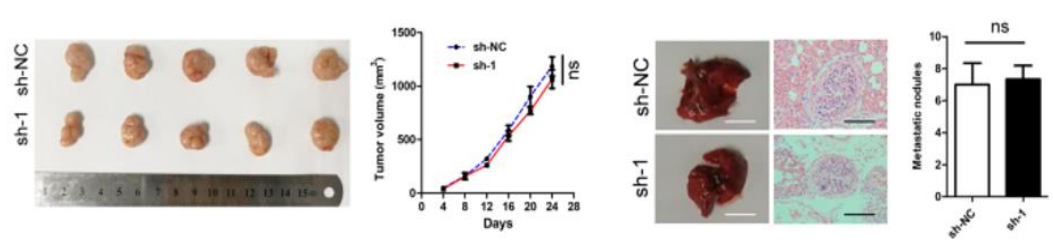

b)

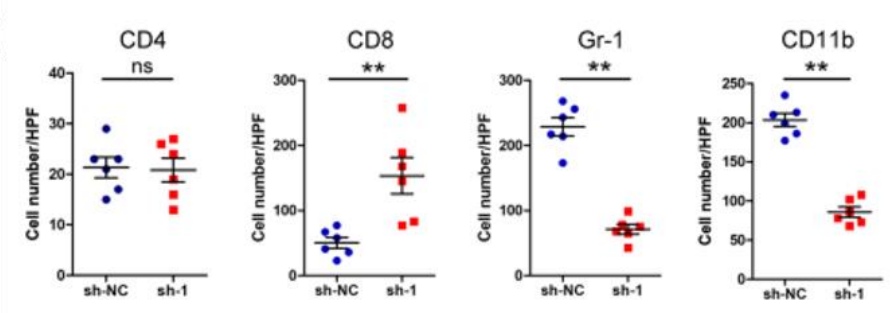

c)

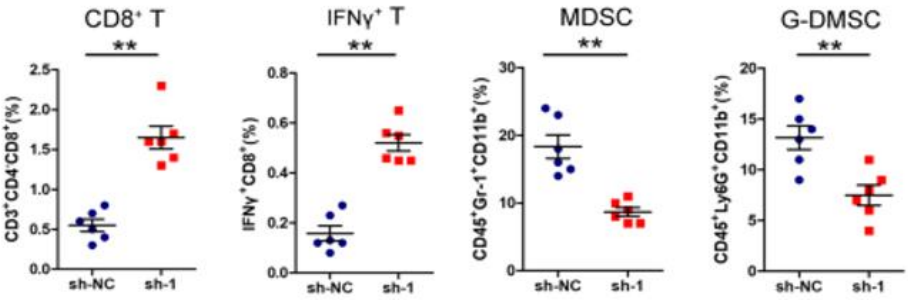

d)

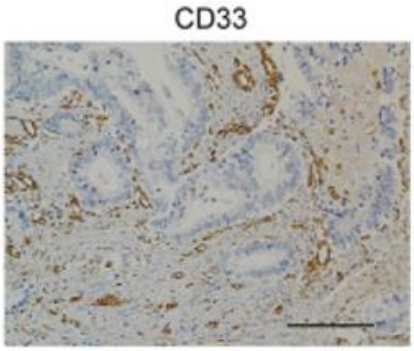

e)

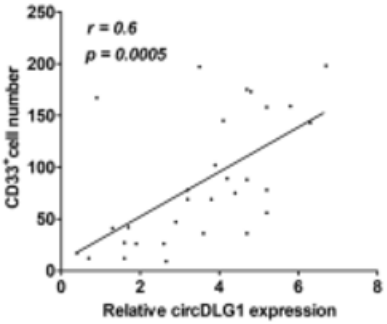

f)

Figure 4. CircDLG1 enhances tumor growth by recruiting MDSCs

a) C57BL/6 mice were injected subcutaneously with either control MFC-sh-NC cells or MFC-sh-circDLG1 cells. Tumor size was measured every four days, and mice were sacrificed at 4 weeks (n = 10 per group). Tumor growth curves indicate that circDLG1 depletion markedly inhibited tumor expansion ($P < 0.05$, two-way ANOVA). Lungs were excised, paraffin-embedded, sectioned (4 μm), and stained with hematoxylin-eosin to visualize metastatic foci. Micrometastasis counts revealed a significant reduction in mice with circDLG1-silenced tumors ($P < 0.05$, Student's t-test). Experiments were repeated three times. Scale bars: left, 5 mm; right, 100 μm. b) BALB/c nude mice were subcutaneously implanted with either MFC-sh-NC or MFC-sh-circDLG1 cells. Tumor growth and lung metastases were monitored as described above. No significant differences were observed in tumor size or metastasis between the groups (ns, two-way ANOVA and Student's t-test, n = 10 per group). Experiments were repeated three times. Scale bars: left, 5 mm; right, 100 μm. **c** IHC staining of subcutaneous tumors was performed to detect CD4, CD8, Gr-1, and CD11b. Gr-1 and CD11b mark murine MDSCs. High-power field (HPF) quantification showed increased $CD8^+$ T cells and decreased MDSC infiltration in circDLG1-silenced tumors ($P < 0.05$, Student's t-test). d Flow cytometry confirmed that circDLG1 knockdown resulted in elevated levels of $CD8^+$ T cells and $IFN\gamma^+$ cells, along with a reduction in total MDSCs and granulocytic (G)-MDSCs ($P < 0.05$, Student's t-test; experiments repeated three times). e IHC of human gastric cancer tissues demonstrated $CD33^+$ MDSC presence. Scale bar, 50 μm. f A

significant positive correlation was observed between circDLG1 expression (qRT–PCR) and $CD33^+$ MDSC infiltration in gastric cancer tissues (n = 30, *P < 0.05, Pearson correlation).

CircDLG1 regulates CXCL12 to promote cancer cell aggressiveness and immune escape

To uncover the molecular mechanisms behind circDLG1-mediated tumor progression, we performed transcriptome profiling in SGC7901 cells transfected with circDLG1-targeting shRNA. RNA sequencing revealed that genes involved in T cell trafficking, EMT, and immune-related pathways were significantly affected. GO enrichment analysis highlighted these processes, while KEGG analysis indicated significant involvement of TNF signaling and PI3K-Akt pathways.

Correlation analysis using circRNA/mRNA microarray data identified CXCL12 as the gene most strongly associated with circDLG1. Notably, RNA-seq demonstrated that CXCL12 expression decreased significantly following circDLG1 silencing. qRT–PCR assays confirmed this reduction in mRNA, whereas ectopic expression of circDLG1 restored CXCL12 levels in gastric cancer cells. Western blot analysis further validated decreased CXCL12 protein levels upon circDLG1 knockdown. Rescue experiments showed that forced circDLG1 expression could counteract the migration defects caused by CXCL12 knockdown. Additionally, circDLG1 levels positively correlated with CXCL12 expression in clinical gastric cancer samples. Collectively, these results suggest that circDLG1 contributes to tumor progression at least partly through CXCL12 upregulation.

CircDLG1 acts as a ceRNA for miR-141-3p to modulate CXCL12

Given its cytoplasmic localization, we hypothesized that circDLG1 might act as a competing endogenous RNA (ceRNA) to sequester miRNAs. Bioinformatic predictions using miRanda and TargetScan identified 46 candidate miRNAs that could interact with circDLG1.

RIP assays in SGC7901 cells expressing Flag-AGO2 demonstrated significant enrichment of circDLG1 in the RNA-induced silencing complex (RISC), indicating its interaction with AGO2 **(Figure 5a).** A luciferase reporter containing a circDLG1 fragment showed decreased activity upon circDLG1 knockdown **(Figure. 5b).** A screen of 46 miRNA mimics revealed that miR-141-3p, miR-138-5p, miR-651-3p, and miR-155-3p could significantly reduce circDLG1 reporter activity **(Figures 5c and 5d).**

Pull-down experiments with a biotin-labeled circDLG1 probe confirmed that miR-141-3p was selectively enriched, whereas the other three miRNAs were not **(Figure 5e).** Knockdown of circDLG1 reduced miR-141-3p enrichment **(Figure 5f),** and an inverse relationship between circDLG1 and miR-141-3p expression was observed in gastric cancer tissues **(Figure 5g).** Finally, RNA FISH demonstrated colocalization of circDLG1 and miR-141-3p in gastric cancer cells **(Figure 5h),** supporting a functional role for circDLG1 as a miR-141-3p sponge that regulates CXCL12 expression.

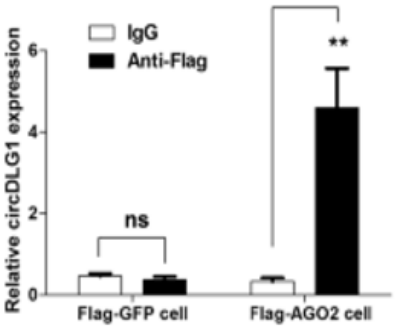

a)

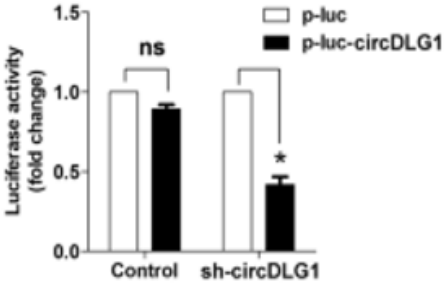

b)

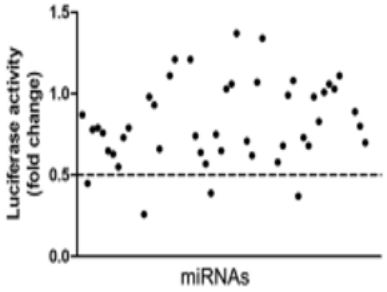

c)

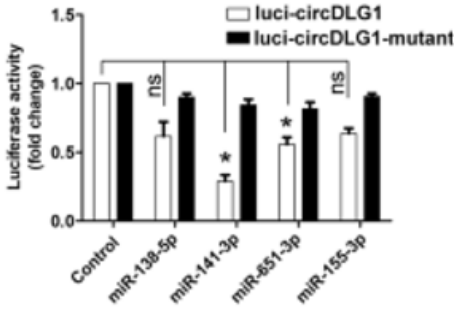
luci-circDLG1
luci-circDLG1-mutant
Luciferase activity (fold change)
1.5
1.0
0.5
0.0
ns
*
*
ns
Control
miR-138-5p
miR-141-3p
miR-651-3p
miR-155-3p

d)

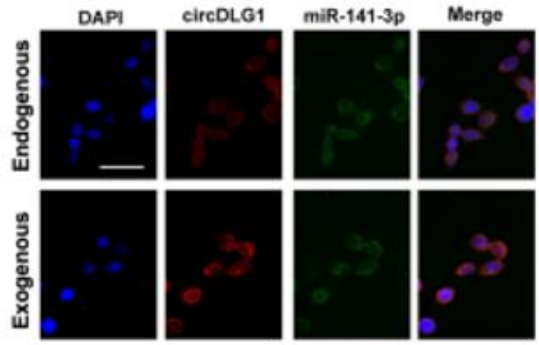
DAPI
circDLG1
miR-141-3p
Merge
Endogenous
Exogenous

h)

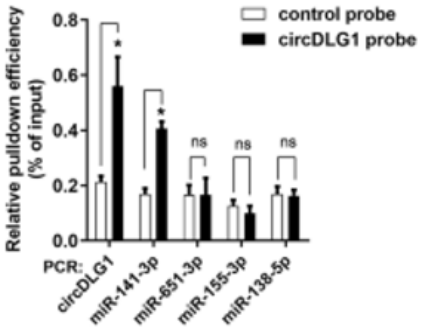
control probe
circDLG1 probe
Relative pulldown efficiency (% of input)
0.8
0.6
0.4
0.2
0.0
*
*
ns
ns
ns
PCR:
circDLG1
miR-141-3p
miR-651-3p
miR-155-3p
miR-138-5p

e)

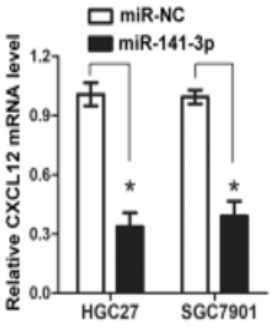
miR-NC
miR-141-3p
Relative CXCL12 mRNA level
1.2
0.9
0.6
0.3
0.0
*
*
HGC27
SGC7901

i)

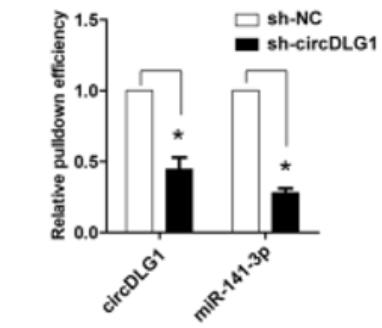
sh-NC
sh-circDLG1
Relative pulldown efficiency
1.5
1.0
0.5
0.0
*
*
circDLG1
miR-141-3p

f)

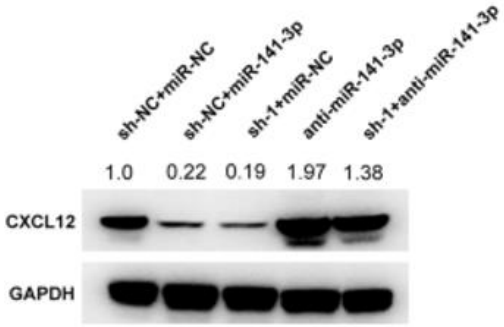
sh-NC+miR-NC
sh-NC+miR-141-3p
sh-1+miR-NC
anti-miR-141-3p
sh-1+anti-miR-141-3p
1.0
0.22
0.19
1.97
1.38
CXCL12
GAPDH

j)

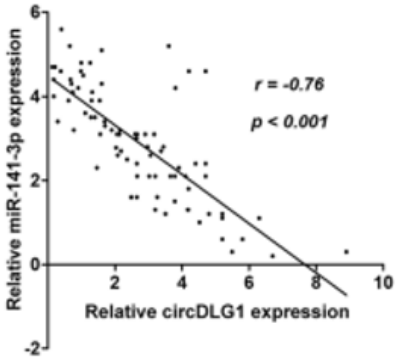
Relative miR-141-3p expression
6
4
2
0
-2
r = -0.76
p < 0.001
2
4
6
8
10
Relative circDLG1 expression

g)

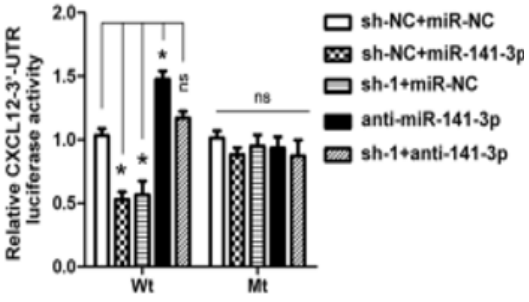
Relative CXCL12-3'-UTR luciferase activity
2.0
1.5
1.0
0.5
0.0
*
*
*
ns
ns
Wt
Mt
sh-NC+miR-NC
sh-NC+miR-141-3p
sh-1+miR-NC
anti-miR-141-3p
sh-1+anti-141-3p

k)

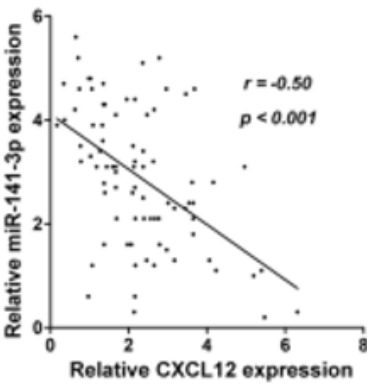

l)

Figure 5. CircDLG1 acts as a miR-141-3p sponge to modulate CXCL12 expression

a RNA immunoprecipitation (RIP) in SGC7901 cells stably expressing Flag-AGO2 or Flag-GFP confirmed significant enrichment of circDLG1 in the AGO2-containing RISC complex ($P < 0.01$, Student's t-test; three independent replicates). b Transfection of circDLG1 shRNA into SGC7901 cells led to a significant reduction in luciferase activity from the circDLG1 reporter construct ($P < 0.05$, Student's t-test; three independent replicates). c-d A luciferase-based miRNA screen was performed using a library of 46 miRNA mimics in SGC7901 cells. Four miRNAs—miR-141-3p, miR-138-5p, miR-651-3p, and miR-155-3p—significantly reduced luciferase activity of the circDLG1 reporter ($P < 0.05$, one-way ANOVA with Bonferroni post hoc test; repeated three times). e-f RIP using a biotin-labeled circDLG1 probe demonstrated that miR-141-3p was selectively enriched ($P < 0.05$, Student's t-test; repeated three times), and this enrichment was reduced when circDLG1 was silenced. g Analysis of 82 gastric cancer tissue samples revealed a strong inverse correlation between circDLG1 and miR-141-3p expression levels (Pearson correlation, $P < 0.001$). h RNA FISH confirmed colocalization of circDLG1 and miR-141-3p in gastric cancer cells (scale bar, 50 μm). i-j Ectopic expression of miR-141-3p significantly reduced CXCL12 mRNA levels ($P < 0.05$, Student's t-test; three replicates), and Western blotting showed that miR-141-3p overexpression or circDLG1 knockdown reduced CXCL12 protein. Inhibition of miR-141-3p increased CXCL12, but this effect was partially reversed by circDLG1 knockdown **(Figure 5j).** k Luciferase reporter assays using wild-type or mutant CXCL12 3′-UTR constructs confirmed that miR-141-3p overexpression or circDLG1 silencing reduced wild-type reporter activity, whereas inhibition of miR-141-3p increased it; no effect was observed with the mutant 3′-UTR ($P < 0.05$, one-way ANOVA with Bonferroni correction; three replicates). l In gastric cancer tissues, miR-141-3p levels were inversely correlated with CXCL12 expression ($n = 82$, $P < 0.001$, Pearson correlation).

These data collectively indicate that circDLG1 can act as a sponge for miR-141-3p, thereby positively regulating CXCL12 expression.

CXCL12 contributes to tumor progression and anti-PD-1 resistance in gastric cancer

CXCL12 has been implicated in tumor growth and immune evasion [35, 36]. To investigate its role in gastric cancer and response to anti-PD-1 therapy, functional experiments were performed. Knockdown of CXCL12 in SGC7901 and HGC27 cells significantly reduced invasive capacity, whereas ectopic CXCL12 expression in AGS cells enhanced invasion .Western blot analysis showed that CXCL12 suppression decreased N-cadherin expression and increased E-cadherin levels, suggesting an effect on EMT.

To examine the impact on anti-PD-1 therapy, MFC-sh-NC or MFC-sh-CXCL12 cells were implanted subcutaneously or via tail vein into C57BL/6 mice. Mice were treated with 0.9% saline, AMD3100 (CXCR4 inhibitor), or anti-PD-1 antibody. CXCL12 knockdown alone significantly inhibited tumor growth and metastasis, and this effect was further enhanced by anti-PD-1 treatment **(Figures 6a and b).** Similarly, AMD3100 treatment suppressed tumor progression, and its combination with anti-PD-1 showed additive inhibition.

Kaplan–Meier analysis revealed that CXCL12 depletion or AMD3100 treatment significantly prolonged overall survival (OS), which was further improved by anti-PD-1 therapy **(Figure 6c).** Flow cytometry of subcutaneous tumors demonstrated that CXCL12 knockdown, AMD3100, and anti-PD-1 therapy increased $CD8^+$ T cells and $IFN\gamma^+$ cells while reducing MDSC populations **(Figures 6d-6f).**

Finally, in gastric cancer patients, high CXCL12 expression was associated with resistance to anti-PD-1 therapy and worse post-treatment survival outcomes **(Figures 6g-6i),** indicating that CXCL12 is a critical mediator of immune evasion and anti-PD-1 resistance

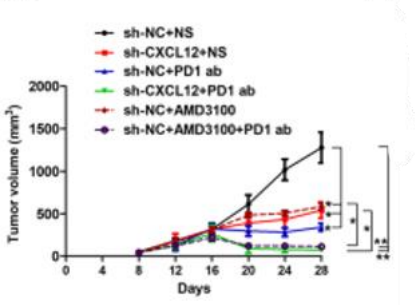
sh-NC+NS
sh-CXCL12+NS
sh-NC+PD1 ab
sh-CXCL12+PD1 ab
sh-NC+AMD3100
sh-NC+AMD3100+PD1 ab
Tumor volume (mm³)
Days

a)

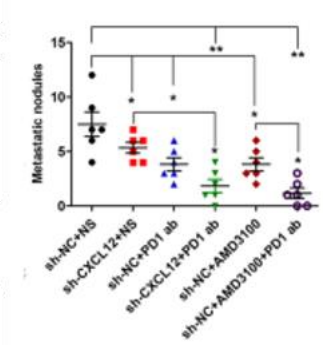
Metastatic nodules
sh-NC+NS
sh-CXCL12+NS
sh-NC+PD1 ab
sh-CXCL12+PD1 ab
sh-NC+AMD3100
sh-NC+AMD3100+PD1 ab

b)

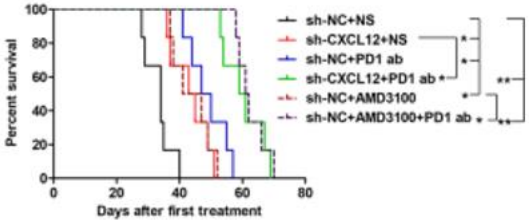
Percent survival
Days after first treatment
sh-NC+NS
sh-CXCL12+NS
sh-NC+PD1 ab
sh-CXCL12+PD1 ab
sh-NC+AMD3100
sh-NC+AMD3100+PD1 ab

c)

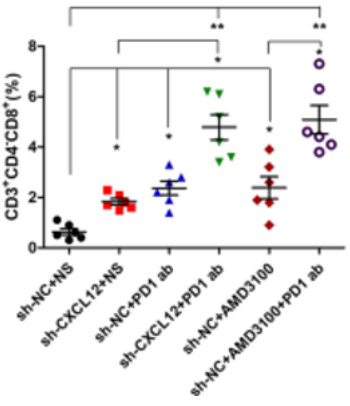
CD3⁺CD4⁻CD8⁺(%)
sh-NC+NS
sh-CXCL12+NS
sh-NC+PD1 ab
sh-CXCL12+PD1 ab
sh-NC+AMD3100
sh-NC+AMD3100+PD1 ab

d)

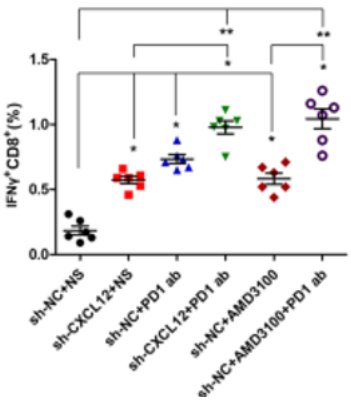
IFNγ⁺CD8⁺(%)
sh-NC+NS
sh-CXCL12+NS
sh-NC+PD1 ab
sh-CXCL12+PD1 ab
sh-NC+AMD3100
sh-NC+AMD3100+PD1 ab

e)

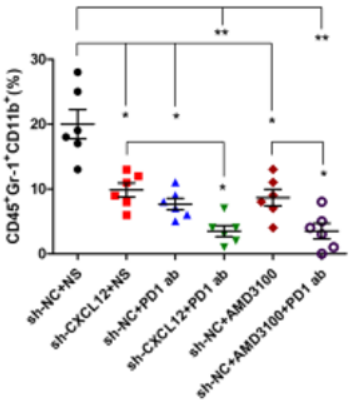
CD45⁺Gr-1⁺CD11b⁺(%)
sh-NC+NS
sh-CXCL12+NS
sh-NC+PD1 ab
sh-CXCL12+PD1 ab
sh-NC+AMD3100
sh-NC+AMD3100+PD1 ab

f)

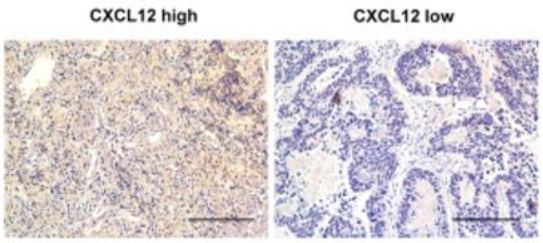
CXCL12 high
CXCL12 low

g)

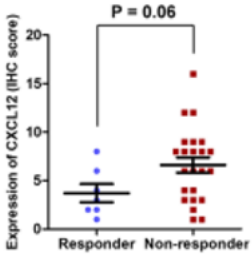
P = 0.06
Expression of CXCL12 (IHC score)
Responder
Non-responder

h)

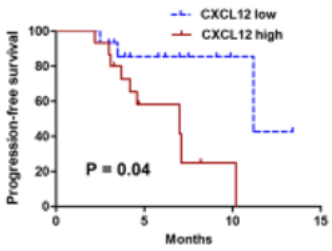

i)

Figure 6. CXCL12 correlates with anti-PD-1 resistance in gastric cancer.

a C57BL/6 mice were subcutaneously injected with different gastric cancer cells and subsequently treated with 0.9% saline (NS), AMD3100 (CXCR4 inhibitor), or anti-PD-1 antibody. Tumor volumes were recorded at specified time points. Statistical significance was assessed using two-way ANOVA with Bonferroni correction for multiple comparisons (*P < 0.05, **P < 0.01*). b Following treatment with NS, AMD3100, or anti-PD-1, the mice were sacrificed, and pulmonary metastatic nodules were quantified. Data were analyzed using one-way ANOVA for multiple group comparisons and Student's t-test for pairwise comparisons, with Bonferroni adjustment where appropriate (*P < 0.05, **P < 0.01*). c Overall survival was estimated using the Kaplan–Meier method, and differences between groups were evaluated using the log-rank test with Bonferroni correction for multiple comparisons (*P < 0.05, **P < 0.01*). d-f Flow cytometry was performed on cells from subcutaneous tumors to determine the frequencies of $CD8^+$ T cells, $IFN\gamma^+$ cells, and MDSCs across treatment groups. One-way ANOVA and Student's t-test were applied as described above, with Bonferroni correction for multiple testing (*P < 0.05, **P < 0.01*). g Representative immunohistochemistry (IHC) image showing CXCL12 expression in human gastric cancer tissues (scale bar, 50 μm). h Correlation analysis between CXCL12 expression and response to anti-PD-1 therapy in patients (Student's t-test, P = 0.06). i Kaplan–Meier survival curves comparing mice with different levels of CXCL12 expression, showing a significant difference in survival (P = 0.04).

Circular RNAs (circRNAs) have increasingly been recognized as important players in a variety of diseases [37, 38]. Many circRNAs exhibit specificity for particular tissues or cell types [39], which points to potential functional significance in cellular processes. Dysregulation of circRNAs has been linked to diverse pathological states, including cardiac hypertrophy, neurological disorders, and cancer [38, 40]. In this study, by comparing circRNA profiles in primary versus matched distant metastatic gastric cancer tissues, as well as in samples from patients who responded or did not respond to anti-PD-1 therapy, we identified **circDLG1** (hsa_circ_0008583) as consistently upregulated in metastatic and therapy-resistant tissues. Clinically, high circDLG1 levels were associated with shorter progression-free survival (PFS) in gastric cancer patients receiving anti-PD-1 treatment, implicating circDLG1 in both tumor progression and immunotherapy resistance.

Functional assays revealed that circDLG1 enhances cellular proliferation, migration, epithelial-mesenchymal transition (EMT), and stemness features. In vivo, circDLG1 promoted tumor growth and metastasis in immunocompetent mice, whereas these effects were absent in immunodeficient models, suggesting that circDLG1 may modulate immune-related mechanisms. Specifically, silencing circDLG1 led to increased infiltration of CD8+ T cells and decreased myeloid-derived suppressor cells (MDSCs), indicating a role in immune regulation. Notably, EMT has previously been implicated in tumor immune escape and resistance to anti-PD-1 therapy [41-43], supporting our finding that circDLG1 orchestrates both EMT and immune evasion in gastric cancer.

Although several biomarkers such as microsatellite instability (MSI), PD-L1 expression, tumor mutation burden (TMB), EBV status, and POLD/POLε mutations have been suggested to predict anti-PD-1 responsiveness [9, 44], reliable predictive markers remain limited. Our previous work indicated that circulating tumor DNA profiles could serve as a potential predictor of immune checkpoint inhibitor efficacy in gastric cancer [45]. In this context, we found that circDLG1 upregulates CXCL12**,** a chemokine previously associated with gastric cancer progression and metastasis [46]. CXCL12 is known to facilitate immune evasion by recruiting MDSCs into the tumor microenvironment [36]. In our experiments, CXCL12 knockdown reduced invasive capacity and improved sensitivity to anti-PD-1 therapy, and CXCL12 levels correlated with PFS in treated patients, consistent with observations in other malignancies [34, 47]. The CXCL12/CXCR4 signaling axis has also been implicated in anti-PD-1 resistance in several cancers [34], and pharmacological inhibition of CXCR4 using AMD3100 has been shown to enhance anti-PD-1 efficacy in melanoma [47]. We further

demonstrated that AMD3100 significantly improved anti-PD-1 responses in gastric cancer models, suggesting that targeting CXCL12 may provide a viable strategy to overcome resistance.

CircRNAs are well-known to act as sponges for microRNAs (miRNAs), thereby influencing protein-coding gene expression. Examples include circACVR2A, which suppresses bladder cancer via the miR-626/EYA4 axis [48], circ-RanGAP1, which regulates VEGFA through miR-877-3p to promote gastric cancer invasion [49], and circCCDC9, which sponges miR-6792-3p to inhibit gastric cancer progression [50]. In this study, circDLG1 was predominantly cytoplasmic, and RNA immunoprecipitation (RIP) and pulldown assays confirmed its interaction with miR-141-3p**.** Luciferase reporter experiments and RNA FISH further validated direct binding and cytoplasmic colocalization, demonstrating that circDLG1 can function as a miRNA sponge to modulate CXCL12 expression.

This study has limitations. The cohort size was relatively small, requiring validation in larger patient populations. CircDLG1 was not detected in plasma, possibly due to RNA degradation over time; further studies should evaluate plasma or exosomal detection. Finally, the mouse models used may not fully replicate the human tumor immune microenvironment, highlighting the need for patient-derived xenograft studies.

Conclusion

We have identified **c**ircDLG1 as a novel circRNA upregulated in metastatic gastric cancer and tissues resistant to anti-PD-1 therapy. Functional analyses revealed that circDLG1 promotes proliferation, invasion, immune evasion, and therapy resistance. Clinically, elevated circDLG1 correlates with poor prognosis in anti-PD-1-treated patients. Mechanistically, circDLG1 acts as a sponge for miR-141-3p, regulating CXCL12**,** which in turn recruits MDSCs and impairs CD8+ T cell function. Overall, our findings highlight the circDLG1/CXCL12 axis as a critical mediator of immune evasion and anti-PD-1 resistance in gastric cancer.

Acknowledgments: We thank all of the patients enrolled in this study.

Conflict of Interest: None

Financial Support: This study was supported by the National Key R&D Program of China (2018YFC1313300); Science and Technology Program of Guangdong (2019B020227002); CAMS Innovation Fund for Medical Sciences (CIFMS) (2019-I2M-5-036); National Natural Science Foundation of China (No.81372570); Natural Science Foundation of Guangdong Province (No. 2014A030312015; No. 2016A030310195); and The Outstanding Youth Cultivation Fund of SYSUCC (No. PT04141002).

Ethics Statement: None

References

1. Sung H, Ferlay J, Siegel RL, Laversanne M, Soerjomataram I, Jemal A, et al. Global cancer statistics 2020: GLOBOCAN estimates of incidence and mortality worldwide for 36 cancers in 185 countries. CA Cancer J Clin. 2021;71(3):209–49.
2. Lu C, Paschall AV, Shi H, Savage N, Waller JL, Sabbatini ME, et al. The MLL1-H3K4me3 axis-mediated PD-L1 expression and pancreatic cancer immune evasion. J Natl Cancer Inst. 2017;109(6):djw283.
3. Vinay DS, Ryan EP, Pawelec G, Talib WH, Stagg J, Elkord E, et al. Immune evasion in cancer: mechanistic basis and therapeutic strategies. Semin Cancer Biol. 2015;35(Suppl):S185–98.
4. Spranger S. Mechanisms of tumor escape in the context of the T-cell-inflamed and the non-T-cell-inflamed tumor microenvironment. Int Immunol. 2016;28(8):383–91.
5. Wu AA, Drake V, Huang HS, Chiu S, Zheng L. Reprogramming the tumor microenvironment: tumor-induced immunosuppressive factors paralyze T cells. Oncoimmunology. 2015;4(7):e1016700.
6. Rizvi NA, Mazieres J, Planchard D, Stinchcombe TE, Dy GK, Antonia SJ, et al. Activity and safety of nivolumab, an anti-PD-1 immune checkpoint inhibitor, for patients with advanced, refractory squamous non-small-cell lung cancer (CheckMate 063): a phase 2, single-arm trial. Lancet Oncol. 2015;16(3):257–65.
7. Ansell SM, Lesokhin AM, Borrello I, Halwani A, Scott EC, Gutierrez M, et al. PD-1 blockade with nivolumab in relapsed or refractory Hodgkin's lymphoma. N Engl J Med. 2015;372(4):311–9.

8. Wang F, Wei XL, Wang FH, Xu N, Shen L, Dai GH, et al. Safety, efficacy and tumor mutational burden as a biomarker of overall survival benefit in chemo-refractory gastric cancer treated with toripalimab, a PD-1 antibody in phase Ib/II clinical trial NCT02915432. Ann Oncol. 2019;30(9):1479–86.
9. Kim ST, Cristescu R, Bass AJ, Kim KM, Odegaard JI, Kim K, et al. Comprehensive molecular characterization of clinical responses to PD-1 inhibition in metastatic gastric cancer. Nat Med. 2018;24(9):1449–58.
10. Davis AA, Patel VG. The role of PD-L1 expression as a predictive biomarker: an analysis of all US Food and Drug Administration (FDA) approvals of immune checkpoint inhibitors. J Immunother Cancer. 2019;7(1):278.
11. Shitara K, Ozguroglu M, Bang YJ, Di Bartolomeo M, Mandala M, Ryu MH, et al. Pembrolizumab versus paclitaxel for previously treated, advanced gastric or gastro-oesophageal junction cancer (KEYNOTE-061): a randomised, open-label, controlled, phase 3 trial. Lancet. 2018;392(10142):123–33.
12. Shitara K, Van Cutsem E, Bang YJ, Fuchs C, Wyrwicz L, Lee KW, et al. Efficacy and safety of pembrolizumab or pembrolizumab plus chemotherapy vs chemotherapy alone for patients with first-line, advanced gastric Cancer: the KEYNOTE-062 phase 3 randomized clinical trial. JAMA Oncol. 2020;6(10):1571–80.
13. Janjigian YY, Bendell J, Calvo E, Kim JW, Ascierto PA, Sharma P, et al. CheckMate-032 study: efficacy and safety of nivolumab and nivolumab plus ipilimumab in patients with metastatic esophagogastric cancer. J Clin Oncol. 2018;36(28):2836–44.
14. Bang YJ, Ruiz EY, Van Cutsem E, Lee KW, Wyrwicz L, Schenker M, et al. Phase III, randomised trial of avelumab versus physician's choice of chemotherapy as third-line treatment of patients with advanced gastric or gastro-oesophageal junction cancer: primary analysis of JAVELIN Gastric 300. Ann Oncol. 2018;29(10):2052–60.
15. Kang YK, Boku N, Satoh T, Ryu MH, Chao Y, Kato K, et al. Nivolumab in patients with advanced gastric or gastro-oesophageal junction cancer refractory to, or intolerant of, at least two previous chemotherapy regimens (ONO-4538-12, ATTRACTION-2): a randomised, double-blind, placebo-controlled, phase 3 trial. Lancet. 2017;390(10111):2461–71.
16. Qu S, Yang X, Li X, Wang J, Gao Y, Shang R, et al. Circular RNA: a new star of noncoding RNAs. Cancer Lett. 2015;365(2):141–8.
17. Jeck WR, Sharpless NE. Detecting and characterizing circular RNAs. Nat Biotechnol. 2014;32(5):453–61.
18. Chen I, Chen CY, Chuang TJ. Biogenesis, identification, and function of exonic circular RNAs. Wiley Interdiscip Rev RNA. 2015;6(5):563–79.
19. Qu S, Zhong Y, Shang R, Zhang X, Song W, Kjems J, et al. The emerging landscape of circular RNA in life processes. RNA Biol. 2017;14(8):992–9.
20. Dong R, Ma XK, Chen LL, Yang L. Increased complexity of circRNA expression during species evolution. RNA Biol. 2017;14(8):1064–74.
21. Ju HQ, Zhao Q, Wang F, Lan P, Wang Z, Zuo ZX, et al. A circRNA signature predicts postoperative recurrence in stage II/III colon cancer. EMBO Mol Med. 2019;11(10):e10168.
22. Thomson DW, Dinger ME. Endogenous microRNA sponges: evidence and controversy. Nat Rev Genet. 2016;17(5):272–83.
23. Zhang Y, Zhang XO, Chen T, Xiang JF, Yin QF, Xing YH, et al. Circular intronic long noncoding RNAs. Mol Cell. 2013;51(6):792–806.
24. Li Z, Huang C, Bao C, Chen L, Lin M, Wang X, et al. Exon-intron circular RNAs regulate transcription in the nucleus. Nat Struct Mol Biol. 2015;22(3):256–64.
25. Liu H, Chen D, Bi J, Han J, Yang M, Dong W, et al. Circular RNA circUBXN7 represses cell growth and invasion by sponging miR-1247-3p to enhance B4GALT3 expression in bladder cancer. Aging (Albany NY). 2018;10(10):2606–23.
26. Rong D, Lu C, Zhang B, Fu K, Zhao S, Tang W, et al. CircPSMC3 suppresses the proliferation and metastasis of gastric cancer by acting as a competitive endogenous RNA through sponging miR-296-5p. Mol Cancer. 2019;18(1):25.
27. Han D, Li J, Wang H, Su X, Hou J, Gu Y, et al. Circular RNA circMTO1 acts as the sponge of microRNA-9 to suppress hepatocellular carcinoma progression. Hepatology. 2017;66(4):1151–64.
28. Hsiao KY, Lin YC, Gupta SK, Chang N, Yen L, Sun HS, et al. Noncoding effects of circular RNA CCDC66 promote colon cancer growth and metastasis. Cancer Res. 2017;77(9):2339–50.

29. Lu YX, Ju HQ, Wang F, Chen LZ, Wu QN, Sheng H, et al. Inhibition of the NF-kappaB pathway by nafamostat mesilate suppresses colorectal cancer growth and metastasis. Cancer Lett. 2016;380(1):87–97.
30. Chen DL, Wang DS, Wu WJ, Zeng ZL, Luo HY, Qiu MZ, et al. Overexpression of paxillin induced by miR-137 suppression promotes tumor progression and metastasis in colorectal cancer. Carcinogenesis. 2013;34(4):803–11.
31. Taki M, Abiko K, Baba T, Hamanishi J, Yamaguchi K, Murakami R, et al. Snail promotes ovarian cancer progression by recruiting myeloid-derived suppressor cells via CXCR2 ligand upregulation. Nat Commun. 2018;9(1):1685.
32. Chen DL, Wang ZQ, Zeng ZL, Wu WJ, Zhang DS, Luo HY, et al. Identification of microRNA-214 as a negative regulator of colorectal cancer liver metastasis by way of regulation of fibroblast growth factor receptor 1 expression. Hepatology. 2014;60(2):598–609.
33. Chen DL, Lu YX, Zhang JX, Wei XL, Wang F, Zeng ZL, et al. Long non-coding RNA UICLM promotes colorectal cancer liver metastasis by acting as a ceRNA for microRNA-215 to regulate ZEB2 expression. Theranostics. 2017;7(19):4836–49.
34. Zeng Y, Li B, Liang Y, Reeves PM, Qu X, Ran C, et al. Dual blockade of CXCL12-CXCR4 and PD-1-PD-L1 pathways prolongs survival of ovarian tumor-bearing mice by prevention of immunosuppression in the tumor microenvironment. FASEB J. 2019;33(5):6596–608.
35. Feng W, Huang W, Chen J, Qiao C, Liu D, Ji X, et al. CXCL12-mediated HOXB5 overexpression facilitates colorectal cancer metastasis through transactivating CXCR4 and ITGB3. Theranostics. 2021;11(6):2612–33.
36. Daniel SK, Seo YD, Pillarisetty VG. The CXCL12-CXCR4/CXCR7 axis as a mechanism of immune resistance in gastrointestinal malignancies. Semin Cancer Biol. 2020;65:176–88.
37. Zhou R, Wu Y, Wang W, Su W, Liu Y, Wang Y, et al. Circular RNAs (circRNAs) in cancer. Cancer Lett. 2018;425:134–42.
38. Shang Q, Yang Z, Jia R, Ge S. The novel roles of circRNAs in human cancer. Mol Cancer. 2019;18(1):6.
39. Chen LL. The biogenesis and emerging roles of circular RNAs. Nat Rev Mol Cell Biol. 2016;17(4):205–11.
40. Arnaiz E, Sole C, Manterola L, Iparraguirre L, Otaegui D, Lawrie CH. CircRNAs and cancer: biomarkers and master regulators. Semin Cancer Biol. 2019;58:90–9.
41. Kolijn K, Verhoef EI, Smid M, Bottcher R, Jenster GW, Debets R, et al. Epithelial-mesenchymal transition in human prostate cancer demonstrates enhanced immune evasion marked by IDO1 expression. Cancer Res. 2018;78(16):4671–9.
42. Hu B, Tian X, Li Y, Liu Y, Yang T, Han Z, et al. Epithelial-mesenchymal transition may be involved in the immune evasion of circulating gastric tumor cells via downregulation of ULBP1. Cancer Med. 2020;9(8):2686–97.
43. Hong W, Xue M, Jiang J, Zhang Y, Gao X. Circular RNA circ-CPA4/ let-7 miRNA/PD-L1 axis regulates cell growth, stemness, drug resistance and immune evasion in non-small cell lung cancer (NSCLC). J Exp Clin Cancer Res. 2020;39(1):149.
44. De Rosa S, Sahnane N, Tibiletti MG, Magnoli F, Vanoli A, Sessa F, et al. EBV^{+} and MSI gastric cancers harbor high PD-L1/PD-1 expression and high $CD8^{+}$ Intratumoral lymphocytes. Cancers (Basel). 2018;10(4):102.
45. Jin Y, Chen DL, Wang F, Yang CP, Chen XX, You JQ, et al. The predicting role of circulating tumor DNA landscape in gastric cancer patients treated with immune checkpoint inhibitors. Mol Cancer. 2020;19(1):154.
46. Izumi D, Ishimoto T, Miyake K, Sugihara H, Eto K, Sawayama H, et al. CXCL12/CXCR4 activation by cancer-associated fibroblasts promotes integrin beta1 clustering and invasiveness in gastric cancer. Int J Cancer. 2016;138(5):1207–19.
47. Wei CY, Zhu MX, Lu NH, Liu JQ, Yang YW, Zhang Y, et al. Circular RNA circ_0020710 drives tumor progression and immune evasion by regulating the miR-370-3p/CXCL12 axis in melanoma. Mol Cancer. 2020;19(1):84.
48. Dong W, Bi J, Liu H, Yan D, He Q, Zhou Q, et al. Circular RNA ACVR2A suppresses bladder cancer cells proliferation and metastasis through miR-626/EYA4 axis. Mol Cancer. 2019;18(1):95.
49. Lu J, Wang YH, Yoon C, Huang XY, Xu Y, Xie JW, et al. Circular RNA circ-RanGAP1 regulates VEGFA expression by targeting miR-877-3p to

facilitate gastric cancer invasion and metastasis. Cancer Lett. 2020;471:38–48.

50. Luo Z, Rong Z, Zhang J, Zhu Z, Yu Z, Li T, et al. Circular RNA circCCDC9 acts as a miR-6792-3p sponge to suppress the progression of gastric cancer through regulating CAV1 expression. Mol Cancer. 2020;19(1):86.